

# Experimental and numerical investigations of aerodynamic characteristics for wind turbine airfoil using multi-suction jets

Ahmed M. Elsayed<sup>a</sup>, Mohamed A. Khalifa<sup>b</sup>, Ernesto Benini<sup>c,\*</sup>, Mohamed A. Aziz<sup>d</sup>

<sup>a</sup> Mechanical Engineering Department, Faculty of Engineering, Fayoum University, 63514, Fayoum, Egypt

<sup>b</sup> Mechanical Engineering Department, Institute of Aviation Engineering and Technology Giza, Egypt

<sup>c</sup> Dipartimento di Ingegneria, Industriale, Università degli Studi di Padova, Via Venezia 1, 35131 Padova, Italy

<sup>d</sup> Mechanical Engineering Department, Faculty of Engineering, Suez University, Suez, Egypt

## ARTICLE INFO

### Article history:

Received 18 January 2023

Received in revised form 8 April 2023

Accepted 10 April 2023

Handling Editor: Jesse L. The

### Keywords:

Active flow control

Continuous suction

Wind turbine blade

Experimental study

Numerical study

## ABSTRACT

The present work investigates the effects of multi-suction jets on the NACA 0012 airfoil's aerodynamic characteristics at Reynolds number  $Re$  equal  $0.54 \times 10^5$ . Experiments and numerical simulations are carried out to this purpose. The surface of the airfoil is equipped with multiple suction slots, and aerodynamic forces are measured as a result. Numerical simulations are employed to illustrate the flow structures on both the modified and unmodified airfoils. The study examines how the lift coefficient, drag coefficient, stall angle, and flow separation are influenced by the location of the airfoil surface suction jets, suction pressure values, and the number of suction slots. Additionally, the study investigates flow reattachments to identify the optimal control case. The results demonstrated that the multiple suction jets along the airfoil blade's upper surface have the best lift coefficient increment performance. In particular, the results showed that maximum improvements in lift coefficient,  $C_L$ , is attained as 480%, at a stall angle of attack (AOA) equal to  $22^\circ$  and flow speed of 8 m/s using numerical simulation with the suction slot. The experimental results showed that lift coefficient improvements,  $C_L$ , reached 55.7% using suction holes at a stall AOA equal to  $16^\circ$  and a flow speed of 8 m/s. In addition, the  $C_L$ ,  $C_D$ ,  $C_L/C_D$ , and separation flow are very sensitive to the suction jet location and the use of the multi-suction technique simultaneously.

© 20XX

## 1. Introduction

The repeated occurrence of severe climates such as storms, extreme floods, heat and cold waves, earthquakes, and biodiversity loss are affecting human life as a result of the abuse and consumption of fossil fuels to an excessive degree. Encouragingly, nearly two hundred countries pledged in 2020 to achieve carbon neutrality by 2050 in an effort to limit global warming to  $1.5^\circ\text{C}$ , a reliable level recommended by the Intergovernmental Panel for Climate Change (IPCC). Carbon neutrality refers to attaining almost zero greenhouse gas emissions and carbon dioxide. Wind, solar, hydro, and further renewable energy are the inevitable means to decrease carbon production. For instance, by the end of 2021, global wind power production capacity has reached 825 GW [1].

NACA airfoils have been used widely in designing Wind Turbines and air vehicles for producing aerodynamic forces with high efficiency. The challenges faced by the designer of such systems stem from the low efficiency of the airfoils under certain flow conditions, such as at high angles of attack, AOA, and at low Reynolds numbers, which lead to stall conditions. In these conditions, in fact, the adverse pressure gradient over the airfoil suction side may prevent reattaching of the separate

flow. Flow separation significantly reduces the lift coefficient and increases the drag coefficient. Several researchers have explored the flow separation and stall occurrences and their impact on aerodynamic properties, specifically in relation to the usability of unmanned aerial vehicles and wind turbines at low Reynolds numbers. This is important to investigate the flow separation and its impact on the aerodynamic properties.

There are two categories for the flow control methods established for a Wind Turbine: active and passive means [2]. The active flow control category, such as suction or blowing or both suction and blowing [3–12] and plasma actuators [13–16], have recently received great attention from researchers. Their functionality can be activated or deactivated based on the actual flow control requirements. In contrast, passive control systems include: slotted airfoils [17–21], vortex generator [22–25], micro-cylinders [26–28], guided vane airfoils [29], leading-edge tubercles [30–33], flaps [34–37], and riblets [38,39]. Such devices do not need supplementary power and have proved their effectiveness in improving aerodynamic characteristics, drag decrease, and power growth. However, passive techniques may introduce unscrupulous drag and noise during operation away from the design conditions.

\* Corresponding author.

E-mail addresses: [ams16@fayoum.edu.eg](mailto:ams16@fayoum.edu.eg) (A.M. Elsayed), [mohamed.khalefa@iaet.edu.eg](mailto:mohamed.khalefa@iaet.edu.eg) (M.A. Khalifa), [ernesto.benini@unipd.it](mailto:ernesto.benini@unipd.it) (E. Benini), [Mohamed.aziz@suezuni.edu.eg](mailto:Mohamed.aziz@suezuni.edu.eg), [Mhessen\\_aziz@yahoo.com](mailto:Mhessen_aziz@yahoo.com) (M.A. Aziz).

<https://doi.org/10.1016/j.energy.2023.127503>

0360-5442/© 20XX

**Table 1**

Summary of previous investigations on the effect of blowing and/or suction jet(s) parameter(s) on the airfoil aerodynamic characteristics.

Ref. No.	Description	Reynolds No.	Method	Studied parameters	Airfoil	AOA range (deg)	Studying blowing and/or suction jet(s) parameter(s)			Meaningful enhancement in the proposed technique	Additional modifications
							Number of jets	Location of jet	operating conditions		
[8]	Numerical simulation	$1 \times 10^6$	blowing	$C_L$ , $C_D$ , and $C_L/C_D$	NACA23012C	0: 24	One blowing	Jet location 20:60% chord	Different velocity $0.5 : 2 V_\infty$	64% increment in lift coefficient Stall AOA delay $2^\circ$	Jet angle $20:60^\circ$
[23]	Experimental investigation	$1.0 \times 10^5$	Individual blowing & suction; combined blowing & suction	$C_L$ and $C_D$	NACA0012	0: 18	One suction One blowing	0.2c, 0.3c & 0.6c	momentum coefficients from 0.026 to 0.418	18.4% increment in lift coefficient Stall AOA delay by $2^\circ$	Not studied
[41]	Numerical simulation	$1.5 \times 10^5$	boundary layer suction	Power coefficient, $C_L$ , and $C_D$	NACA-021 series airfoils	0:26	One suction on each side	Single suction slots from 0.3 to 0.7 chord	constant suction momentum	Power coefficient maximum by 0.55	Changing the maximum thickness position
[42]	Numerical simulation	$1.5 \times 10^6$	blowing and suction	$C_b$ , $C_p$ , and $C_L$	Clark-Y	Only zero	Two blowing and two suction	Fixed, not studied	Fixed, not studied	10% increment in lift coefficient	Not studied
[43]	Numerical simulation	$5 \times 10^5$	blowing and suction	$C_p$ , $C_L$ , and $C_D$	NACA0012	Only 18	One blowing and suction	From 0.03 to 0.8 chord	Different amplitude of velocity From 0.01 to $0.5 V_\infty$	50% increment in lift coefficient	Changes the jet angle $-90$ to $90$ deg
[46]	Numerical simulation	$5 \times 10^5$	Suction	$C_p$ , $C_L$ , $C_L/C_D$ , and $C_D$	NACA0012	0: 22	One suction	Fixed, not studied	Fixed, not studied	30% increment in lift coefficient	Cavity on the airfoil suction surface
[47]	Numerical simulation	$5 \times 10^5$	suction and blowing	$C_L$ , $C_D$ , and $C_L/C_D$	NACA0012	0: 22	One suction One blowing	Fixed, not studied	Three jet velocity ratios and three jet angles	Lift to drag ratio equals 73.7 Increasing in stall angle from $14^\circ$ to $20^\circ$	With/without flap three flap deflections (df)
[48]	Numerical simulation	$1.3 \times 10^5$	co-flow jet	$C_p$ , $C_L$ , and $C_D$	four airfoils NACA0012, 0015, 0018, and 0021	0: 18	One blowing One suction	Fixed, not studied	momentum coefficients of 0.03, 0.05, and 0.08	280% increment in lift coefficient	Not studied
[49]	Large eddy simulation	$2 \times 10^5 : 1 \times 10^7$	blowing and suction	$C_L$ and $C_D$	NACA4412	Only 5	One suction slot One blowing slot	One suction length $(0.25 < x/c < 0.86)$ Different blowing length	Different velocity 0.1 and $0.2 V_\infty$	7% increment in lift coefficient	Not studied
[53]	Numerical simulation	$5 \times 10^5$	suction jet	$C_L$ , $C_D$ , and $C_L/C_D$	NACA0012 3D wing	12:18	One suction	Fixed, not studied	momentum coefficients from 0.00078 to 0.00625	122% increment in lift-to-drag ratio	Spanwise jet location study
Current study	Experimental and Numerical simulation	$1.09 \times 10^5$	suction	$C_p$ , $C_L$ , $C_L/C_D$ , and $C_D$	NACA0012	0: 26	Multi suction jets	Six hole's locations	Different suction pressures From 0 to $-1400$ Pa	480% increment in lift coefficient	Effect of applying one, two, four, and six jets

Suction and blowing are the most utilized selection in the active flow control methods for Wind Turbines. Strict suction has been considered the most important method for controlling flow for a long time. For instance, lift improvement and transition delay are helpful in controlling flow separation and enhancing the airfoil lift-to-drag ratio. The primary objective of the associated research paper was to modify the boundary layer's momentum in order to improve Wind Turbine aerodynamic characteristics. Wang et al. [40] have experimentally investigated the aerodynamic performance of a NACA0012 airfoil using suction and blowing jets at a Reynolds number equal to  $1.0 \times 10^5$ . They concluded that the suction effect the reattachment of flow and thus controls the reattachment position and the separation bubble size. Sun et al. [41] have studied the influence of boundary layer suction position on the aerodynamic characteristics of a NACA-0021 airfoil. According

to their findings, the influence of suction position is determined by separation point variation, while the optimal suction point for the highest lift-to-drag ratio shifts towards the trailing edge. Ohashi et al. [42] have performed numerical simulations for flow around a Clark-Y airfoil using uniform blowing and suction, indicating an improvement in the airfoil's aerodynamic characteristics. Their results showed improvement in the lift-to-drag ratio by applying suction on the upper surface while suction on the lower surface deteriorates it.

Huang et al. [43] simulated the blowing and suction control by placing a jet on a NACA0012 airfoil's upper surface under a Reynolds number equal to  $5 \times 10^5$  and an AOA of  $18^\circ$ . Their results indicated that suction takes advantage of producing a greater and smaller pressure coefficient region on the airfoil's upper surface and hence increases the lift coefficient while the flow is further attached, and the profile drag re-

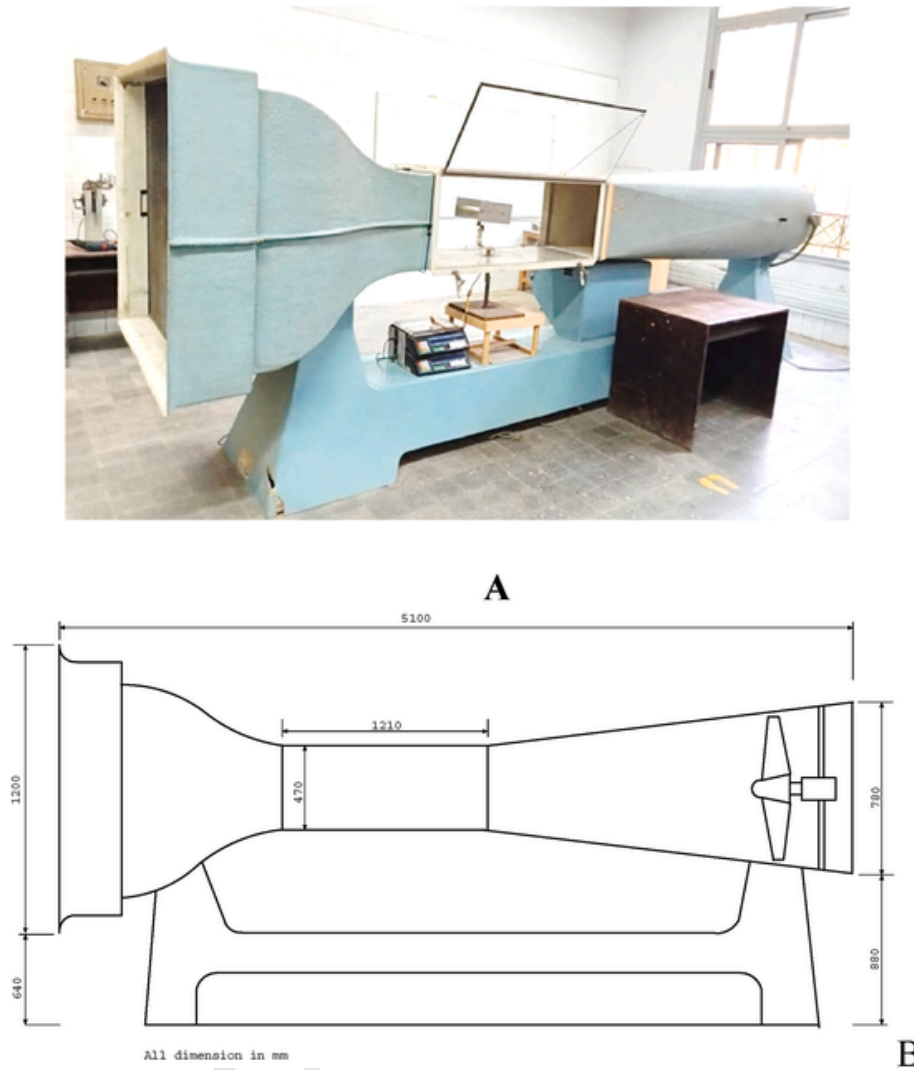


Fig. 1. A Wind tunnel of variable speed 0–35 m/s, and B 2D CAD drawing for the wind tunnel facility including main dimensions.

duces. Sogukpinar et al. [44] have numerically investigated the aerodynamic performance of a NACA 0012 airfoils with varying thicknesses on the pressure side to achieve a high lift coefficient. Gul et al. [45] have experimentally investigated the effect of a controlled synthetic jet using actuators on the aerodynamic performance of the flow within the separation and reattachment regimes. The synthetic jet had eliminated the separation bubble over the airfoil's suction surface at laminar flow with a Reynolds number equal  $2.3 \times 10^5$  at an AOA of zero degrees. Fatahian et al. [46] have investigated numerically the effect of suction and cavity applied on a NACA 0012 for controlling flow separation. According to their findings, the flow control improved the lift-to-drag ratio, and stall AOA was delayed by  $8^\circ$ . Fatahian et al. [47] have compared, using computational fluid dynamics (CFD), the effect of suction and blowing jets on the aerodynamic characteristics of airfoils. Based on their results, the higher suction velocity had the greatest impact on the aerodynamic characteristics of the airfoil. Bak Khoshnevis et al. [48] have investigated the effect of the co-flow jet (CFJ) on the aerodynamic characteristics of symmetric airfoils. Their results indicated a higher lift coefficient and a clear influence on stall angle delaying. Atzori et al. [49] numerically studied the effects of uniform suction and blowing on the aerodynamic performance of a NACA4412 airfoil at a Reynolds number equal  $2 \times 10^5$ . They concluded that uniform suction applied at the suction side improves the aerodynamic performance due to the combined effect of suction on pressure, skin friction drag, and

lift. Arunraj et al. [50] have tried to improve the lift coefficient by using suction at different points to delay boundary layer separation. Zahedi et al. [51] have invested in the load management effect of the wind power plant. Zahedi et al. [52] have studied numerically and investigated experimentally the gas and liquid in ninety-degree elbow.

Table 1 lists and presents previous research on the utilization of suction and blowing for the purpose of regulating the aerodynamic behavior of airfoils. The current study evaluates Wind Turbine airfoils' performance using suction only to demonstrate its effect. The study includes changing the location, the number of suctions, and the suction pressure. A few researchers were exposed to changing the number of suction points detailed in the current study at different AOA. This is followed by the selection of the best cases for study and experimental verification of the success of the proposed aerodynamic control technique. The current work presents the problem statement, and a summary of previous investigations on the effect of blowing and/or suction jet(s) are tabulated in Table 1. A system design and experimental procedure are presented with the model geometry construction, boundary conditions, computational grid sensitivity, and resolution analysis. The results include a validation of the numerical model with current and previous experimental results. A parametric study on slot location, numbers, and suction pressure is simulated numerically using a CFD code. Finally, experimental results on Continuous Suction based on nu-

**Table 2**  
Measuring devices characteristics.

No.	Device	Specification
1	Pitot tube anemometer	Measuring Ranges 1–80 m/s 3.6–288 km/h Air Volume: 0 to 99, 999 (CFM/CMM) Temperature: 32–122 °F (0–50 °C) Accuracy $\pm 2.5\%$ rdg. Air Volume: $\pm 1\%$ FS Temperature: $\pm 1.5$ °C (3 °F) Resolution 0.01 m/s 0.1 km/h 0.001 CFM/CMM 0.1 °F/°C Display 5-digit, Dual LCD Display Interface USB Operating conditions 0 °C–50 °C/<80% Hr. Power 9 V battery Auto shut-off Yes, Yes (after 20 min) Dimensions 210 × 75 × 50 mm Brand Name: Greisinger GMH Power supply 9 V battery, DC. (details) Connector Analogue outputs: 0–1 V Technical Specifications Print resolution 0.1 mbar Accuracy 0.1% Reading range –0.01 bar (min.) Sensor Piezo Resistive pressure sensor internal
2	Digital manometer	
3	Measuring angle	Dimensions (L x W x H) 142 × 71 × 26 mm Resolution 1° Reading range 360° Sensor analog Adjusting manual
4	Lift and drag measuring device	Resolution 1 g Reading range 40 kg Sensor Load cell Accuracy 0.7%

**Table 3**  
Pressure Data Logger specifications.

Device	Measured quantity	Resolution	range	Sample rate	Accuracy
Track-It Data Logger (Pressure 350 D)	pressure	0.014 psi	0:350 psi	10 Samples/s	$\pm 0.25\%$ reading

merical simulation recommendations are compared to the original airfoil.

## 2. System design and experimental procedure

The present setup is conceived for measuring lift and drag forces on a NACA0012 airfoil. A wind tunnel of 50 × 50 cm test section with a variable speed of 0–35 m/s is used, as shown in Fig. 1. The experimental setup features a smooth airfoil of NACA 0012 (original and modified with surface suction jets), a lift and drag forces measuring device in the range 0–40 kg, a negative pressure suction chamber, measuring instruments (velocity and pressure), and an electric control unit. A centrifugal air blower driven by an electric motor of 900 W capacity is used to supply the section chamber with negative pressure of 0.1 bar. The suction distributor is located between the airfoil ports and the negative pressure chamber. Additionally, the velocity is measured using a Pitot tube anemometer. The experimental work is carried out at an air speed of 8 m/s ( $Re = 1.09 \times 10^5$ ), and by varying the AOA in the range 0–24 deg.

Tables 2 and 3 summarize the general specifications of the used measuring devices. The used Pitot tube anemometer and differential manometer provide accurate air velocity, airflow, and ambient air temperature measurements.

Fig. 2 shows the two airfoils used of 20 cm cored and 20 cm length of NACA0012. The first represents the original airfoil, while the second is modified with suction jets through six suction lines connected to the suction chamber via an electrical solenoid gat. A digital manometer was used to measure the pressure drop within the suction lines. The suctioning procedure maintained suction at specific suction locations.

## 3. Numerical modeling and simulations

### 3.1. Governing equations

The Navier-Stokes equations of motion for a compressible flow is a vector equation given by

$$\rho \frac{D\vec{V}}{Dt} = -\vec{\nabla}P + \vec{F} - \vec{\nabla} \times \left[ \mu \left( \vec{\nabla} \times \vec{V} \right) \right] + \vec{\nabla} \cdot \left[ \left( \zeta + \frac{4}{3}\mu \right) \vec{\nabla} \cdot \vec{V} \right]$$

The energy equation is given by

$$\frac{\partial Q}{\partial t} + \Phi + \vec{\nabla} \cdot (k \vec{\nabla} T) - \vec{\nabla} \cdot \vec{q}_r = \rho \frac{De}{Dt} + P \vec{\nabla} \cdot \vec{V}$$

### 3.2. Problem statement and assumption

In the current study, the proposed concept works on boundary layer suction, which prevents the boundary layer flow from slowing down. The elimination of the slowed boundary layers by active suction stabilizes the flow velocity of the boundary layer and eventually retains a laminar boundary layer. Fig. 3 demonstrates the working concept of boundary layer suction. Therefore, the air near the airfoil walls has low energy. The suction of this layer makes the air more stable on the surface of the airfoil. The presence of suction affects the boundary layers and prevents air movement from being reflected, causing reverse flow and, consequently, stall.

### 3.3. Model geometry construction and boundary conditions

Numerical simulations were performed using a commercial Navier–Stokes flow solver. This package has been used in many different applications in the field of Wind Turbines [54], turbomachines [55–58], internal channel flows [59–61] and thermofluidics [62]. Three modules from the solver package were used during the study. The geometry and grid generation was conducted in the CFD-GEOM module, whereas CFD computations were performed in the CFD-ACE module. The postprocessing was conducted in the CFD-VIEW module. Most of the modules are controlled using Python script files. The CFD-ACE multi-physics module is a pressure-based solver. The code solves the time-dependent, Reynolds-averaged Navier–Stokes equations using finite volume, structured grids for turbulent, compressible flows. Spatial accuracy is nominally second-order upwind formulation. The standard k-ε model has been used during the current study based on the recommendation in Refs. [63–65].

Fig. 4 (A) presents the problem's computational domain, defined by a far-field boundary extended from 8 chord lengths upstream to 16 times chord lengths downstream of the airfoil. The downstream length behind the airfoil has been doubled to include the rear vortices due to airflow separation at high AOA. Fig. 4 (C) shows the suction slot (holes) locations considered during the current study. The first slot was located at 0.2 C from the leading edge, and the distance between slots was kept equal to 0.1 C. The slot width was considered equal to 2 mm with a right axis angle to the airfoil surface. The holes were numbered from 1

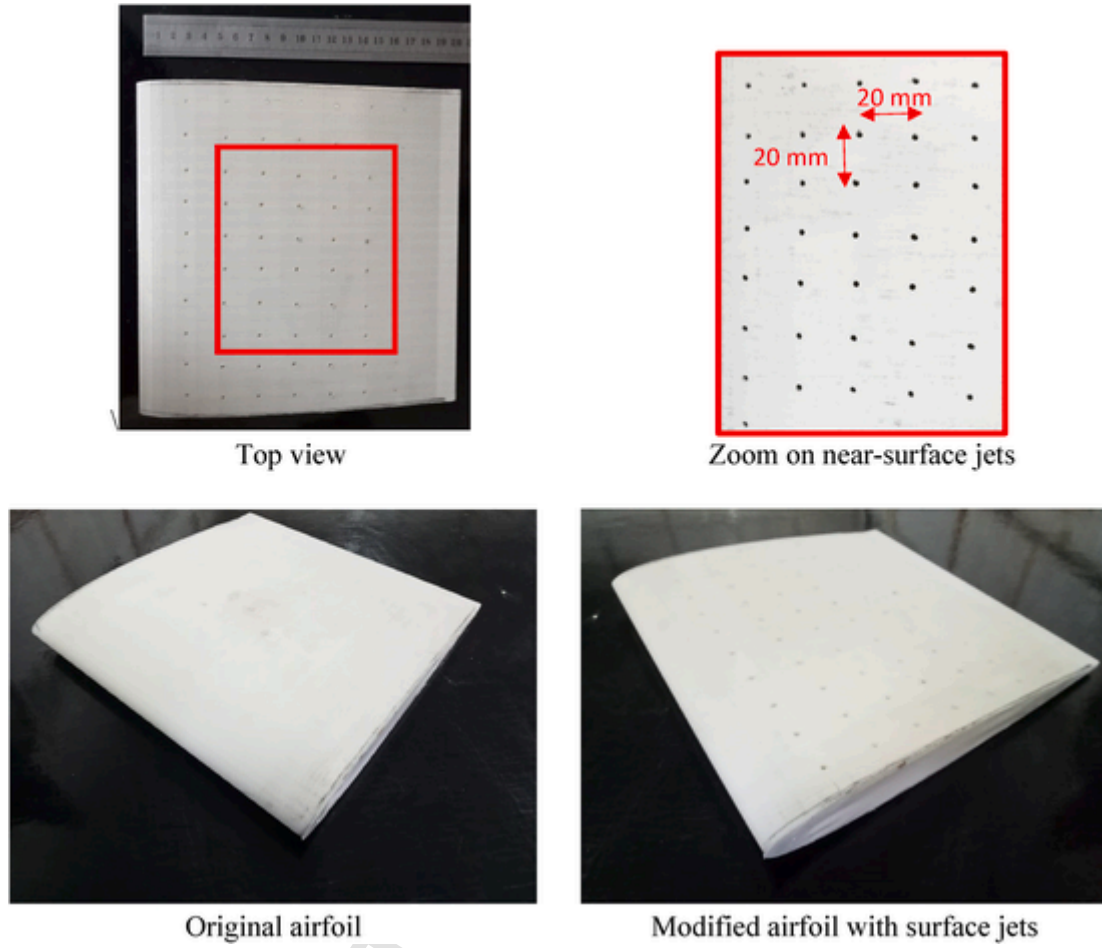


Fig. 2. The modified and original NACA0012 airfoils.

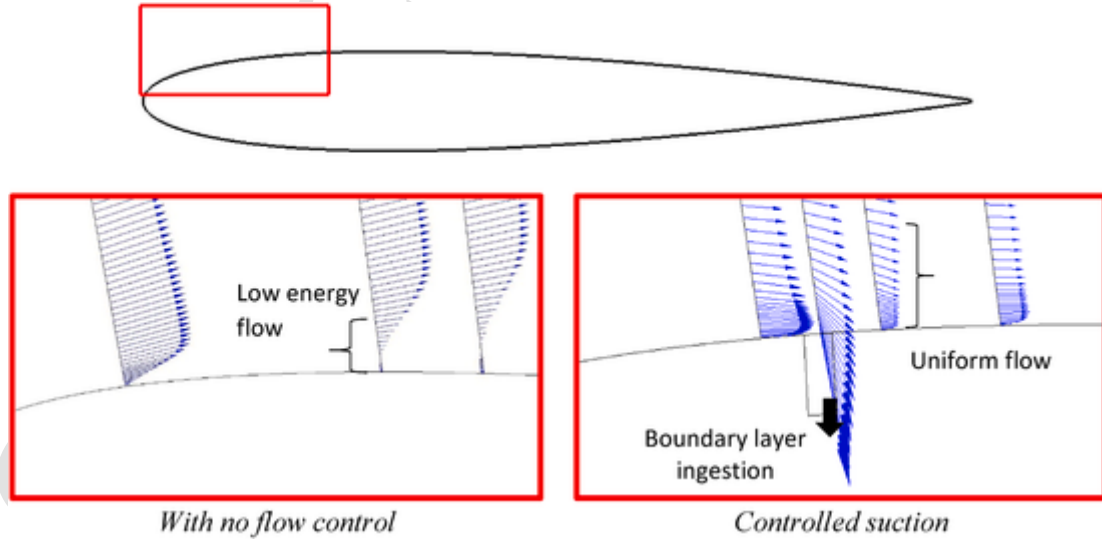


Fig. 3. Effect of suction flow on velocity profile near separation bubble.

to 6 from leading edge to trailing edge to identify them, as demonstrated in Fig. 4 (C). The boundary conditions were defined in Fig. 4 (B). The inlet flow is defined by sea level condition  $P_a$ ,  $T_a$ , free stream velocity,  $V_\infty$ , equal to 8 m/s ( $Re = 1.09 \times 10^5$ ) with different AOA ranging from 0 to  $24^\circ$ . The outlet flow is defined by fixed pressure with



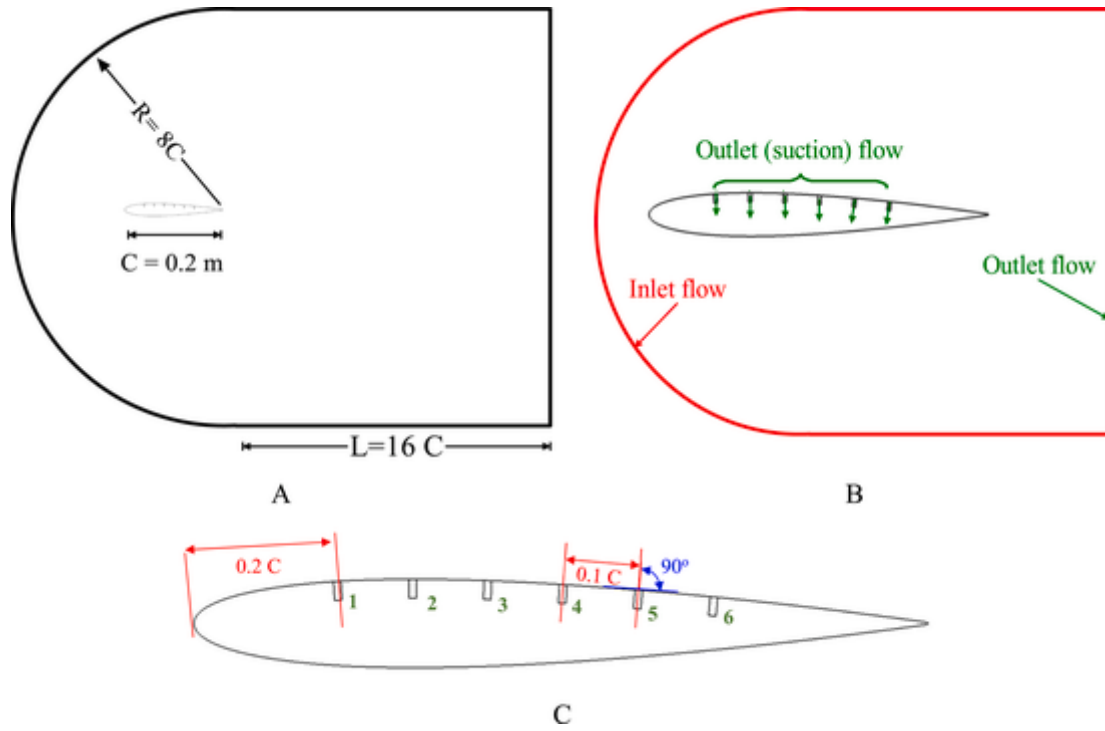


Fig. 4. (A) Airfoil control volume, (B) boundary conditions, and (C) zoom-in suction space definitions.

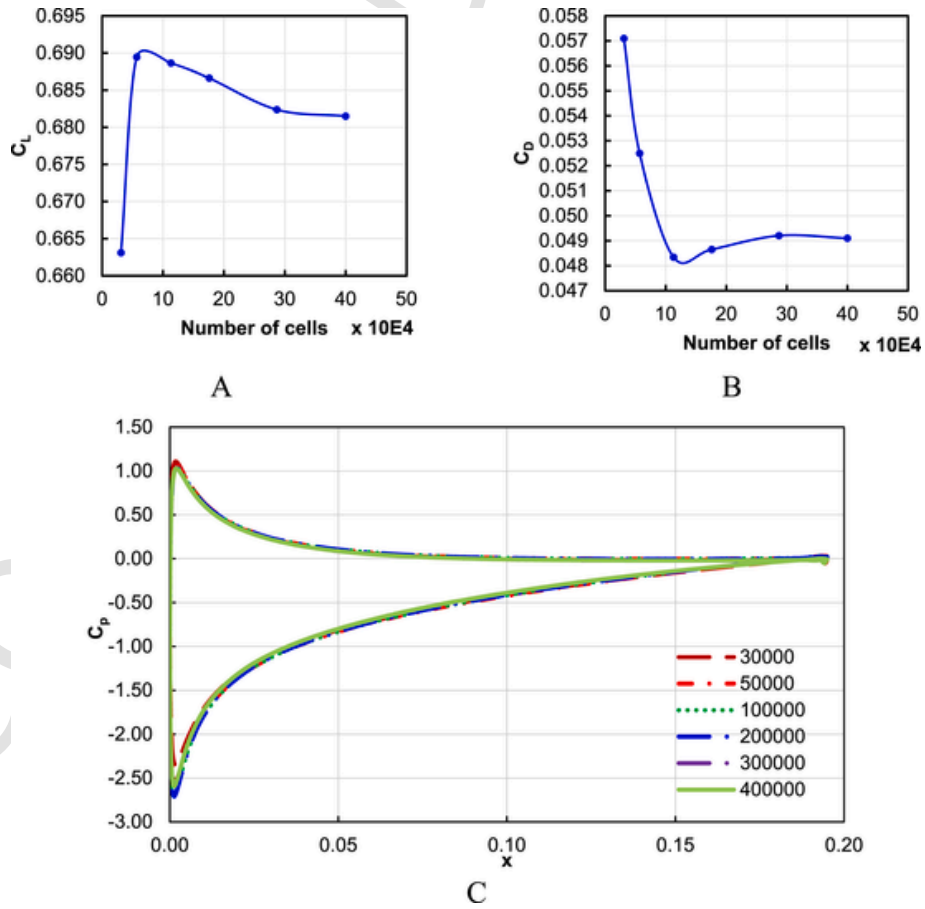


Fig. 5. (A) Lift coefficient, (B) drag coefficient, and (C) pressure coefficient versus grid number at AOA = 8 deg.

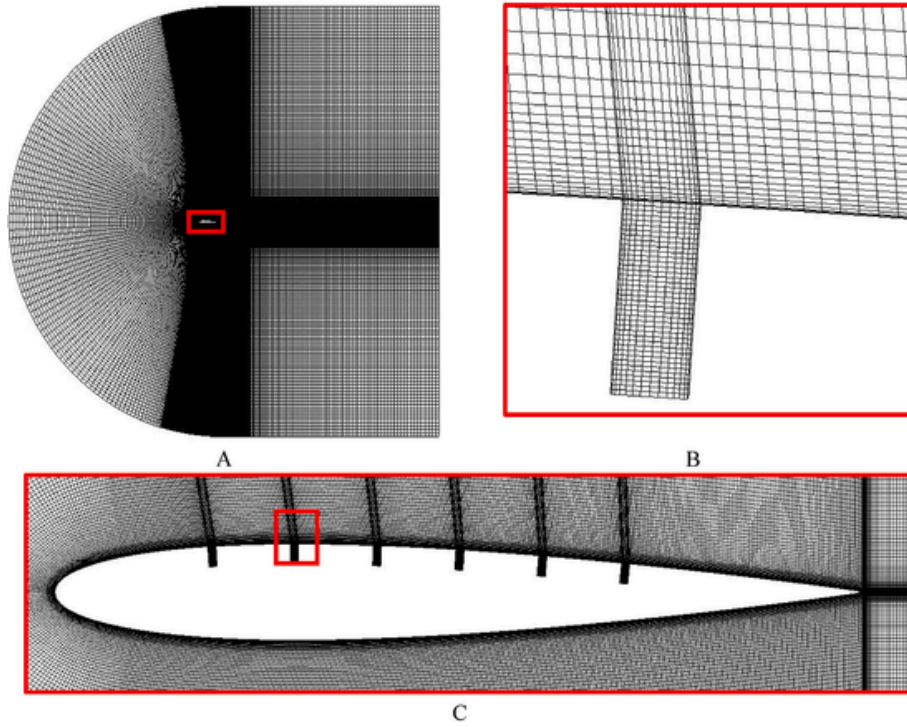


Fig. 6. (A) Control volume structure grid, (B) zoom in hole grid, and (C) zoom in airfoil grid.

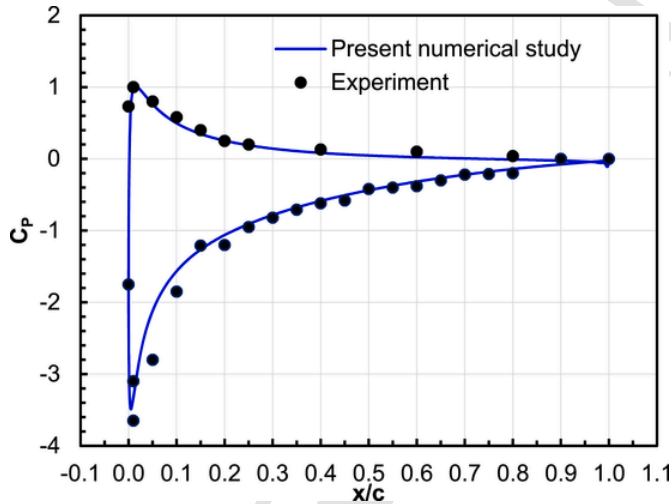


Fig. 7. Comparison of pressure coefficient with experimental data Rinoie et al. (2009) [66] at AOA = 10°.

sea-level conditions. The outlet suction flow is specified with vacuum pressure varying from 200 Pa to 1400 Pa.

### 3.4. Grid resolution and validation of the numerical model

In the current work, for the uncontrolled airfoil, an H-type structured grid is used. A clustered grid is located near the walls to take the boundary layer effect and minimize the  $y^+$  value below 2. A grid-independent study was performed for different grid numbers from 30,000 to 400,000 cells. The results were presented in global calculated parameters  $C_L$ ,  $C_D$ , and local computed parameters  $C_p$  distribution to ensure that the accuracy of the computational grid is sufficiently fine to capture the delicate and important phenomena in the problem. The results showed no change in the values of  $C_L$  and  $C_D$  by increasing the number of cells above 300,000. In addition, there was no change in the

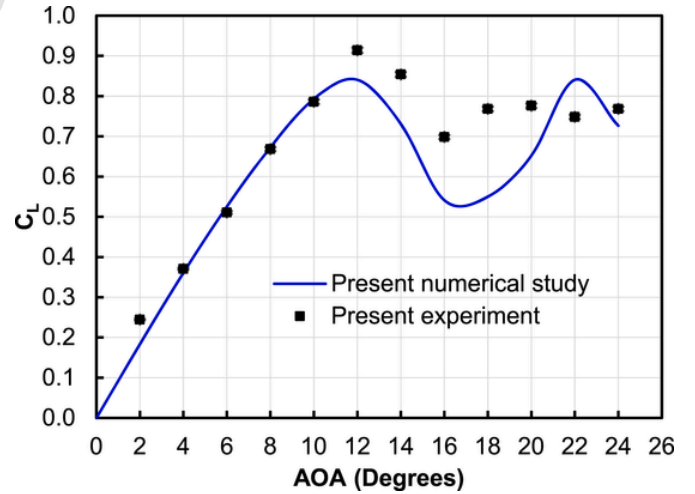


Fig. 8. Comparison of lift coefficient with presented experimental measurement.

values of the pressure coefficient distribution around the airfoil surface. Thus, 300,000 cells were considered a sufficient grid number to simulate the problem correctly. The observed flow field variable, such as  $C_L$  and  $C_D$ , varies with the grid number until the asymptotic numeric value is reached, as shown in Fig. 5.

The best grid number that was achieved to simulate the problem with high accuracy is described in Fig. 6. Fig. 6 (B) shows the quality of the mesh inside the air suction slots, whereas Fig. 6 (C) demonstrates the fineness of the mesh near the airfoil walls.

Prior to applying the numerical simulation with the CFD solver to evaluate the problem, the results of the solver must be validated. Fig. 7 depicts the comparison of the  $C_p$  distribution between the clean airfoil and experimental results by Rinoie et al. (2009) [66] at AOA = 10°. The results obtained agree with the experimental results. A comparison of  $C_L$  with present experimental data is also conducted for the clean air-

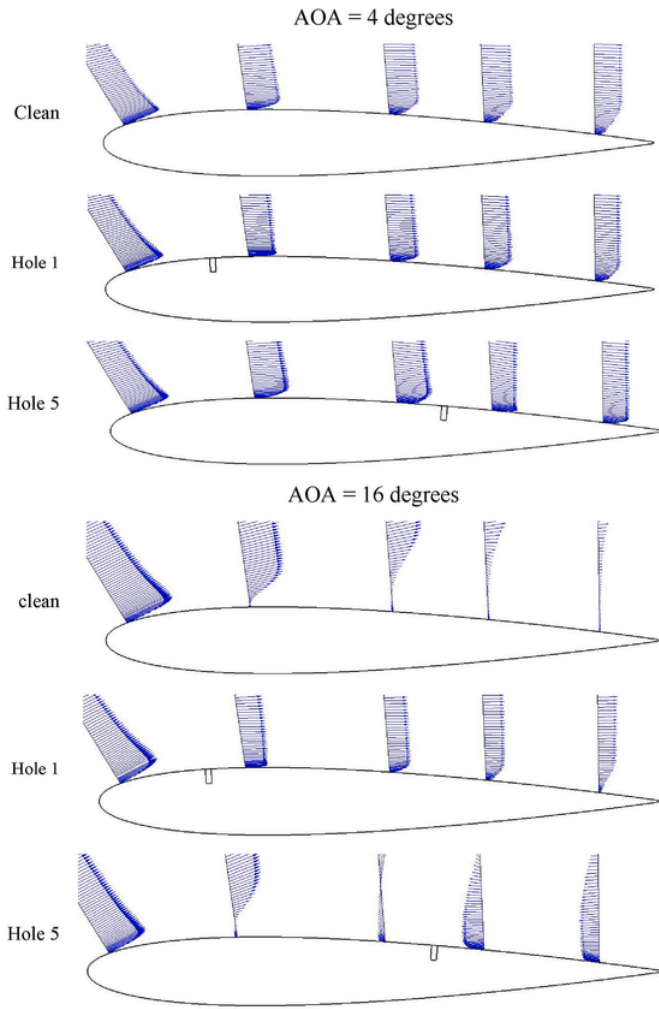


Fig. 9. Effect of hole location on boundary layer.

foil at  $Re = 1.09 \times 10^5$ . Fig. 8 demonstrates the lift coefficient variation with AOA. The results are very similar, up to  $\alpha = 10^\circ$ . The stall angle envisaged by the numerical simulation equals  $12^\circ$  is in excellent agreement with the present experimental data.

#### 4. Experimental and numerical results

##### 4.1. Effect of suction jets location

According to Fig. 9, at small angles of attack, the closeness of the suction distance from the leading edge of the airfoil works to the proximity of the suction distance to the leading edge of the airfoil helps to maintain a more uniform flow without a distinct reverse flow along the upper airfoil surface. However, this effect diminishes as air approaches the airfoil's trailing edge. In contrast, the proximity of the suction slot to the trailing edge of the airfoil only enhances the boundary layer growth near the airfoil leading edge, improves the flow attachment to the airfoil surface, and eliminates flow separation, thus delaying the stall AOA. Conversely, placing the suction slot near the airfoil's trailing edge did not effectively prevent separation.

Fig. 10 (A) shows the variation of the lift coefficient with the AOA at different suction locations. The results presented clearly demonstrate the effectiveness of suction at different locations on the airfoil when compared to the clean airfoil. Among the different suction locations tested, the best results were obtained from suction at hole 6, with a lift coefficient of up to  $14^\circ$  AOA. This is consistent with the previous paragraph's discussion of suction near the airfoil's trailing edge,

where separation begins at low angles of attack. Hole 2, on the other hand, had a larger lift coefficient because, as the angle of attack increases, the separation moves towards the leading edge. Thus, locating the suction closer to the leading edge of the airfoil is preferable. This is further supported by the superior performance of suction at hole 6 at the highest angles of attack, where the separation is very close to the airfoil's leading edge. With regards to stall angle of attack, hole 1 exhibited the best performance, while hole 4 was the worst. Suction at hole 2 also achieved the highest lift coefficient of 2.03 at an angle of attack of  $18^\circ$ .

Fig. 10 (B) shows the airfoil's drag coefficient change with AOA at different suction locations. The total drag is the sum of skin friction drag and pressure drag due to separation. Suction flow reduces the separation, increasing skin friction drag and reducing pressure drag due to separation. It is evident from the results that the value of the drag coefficient deteriorates in the suction locations from 2 to 6. While suction location 1 maintains the drag coefficient values very close to the clean airfoil. The explanation is that as the velocity profile is folded over the largest possible distance on the airfoil (suction location 1), the accompanying shear forces become greater. At large AOA, drag due to pressure decreases due to separation prevention.

Fig. 10 (C) is the true criterion for balancing the values of the lift coefficient and the drag coefficient. According to the results obtained, the value reaches about 80 at an AOA of  $8^\circ$  associated with the 1st suction location instead of 13.2 in the case of the clean airfoil at the same AOA.

Fig. 11 shows the velocity contour around the airfoil for the angles of attack 8, 16, and  $20^\circ$ , respectively. The reason for choosing the angles of attack values used in this study is because separation from the airfoil surface can occur at those angles. The results show that changing the suction location had a significant impact. Suction locations 1, 2, and 3 successfully reattached a significant amount of air along the airfoil surface due to the proximity of the suction to the airfoil leading edge. However, in suction locations 4, 5, and 6, severe separation from the airfoil surface was observed at angles of attack of  $18^\circ$  and  $20^\circ$ , indicating that suction from positions near the trailing edge of the airfoil is ineffective. Fig. 12 illustrates the pressure coefficient ( $C_p$ ) for both the clean airfoil and the controlled suction case at angles of attack of 8, 16, and  $20^\circ$ . The results indicate that abrupt variations in pressure coefficient were detected at various suction locations, which had a positive effect on enhancing aerodynamic coefficients such as lift coefficient and lift-to-drag ratio. The pressure coefficient at the suction location was slightly dependent on the angle of attack, but its stability (constant value) was observed in all studied cases due to its direct relationship with the drag pressure.

The distribution of pressure coefficient along the pressure side of the airfoil remained unchanged despite the alteration in suction location. At suction locations 1 and 2, an increase in angle of attack leads to a rise in the stagnation pressure coefficient near the airfoil's leading edge. This increase is advantageous as it aids in processing the separation bubble in areas near the leading edge of the airfoil. At suction locations 3 and 4, the stagnation pressure coefficient remained stable even at high angles of attack, which indicates that the separation bubble was controllable at the given angle of attack. At suction locations 5 and 6, the stagnation pressure coefficient remained unchanged, but its value was lower compared to other suction locations. This can be explained by the suction's inability to manage the separation on the airfoil surface since the separation began to occur at angles of attack ranging from  $8^\circ$  to  $20^\circ$ .

##### 4.2. Effect of suction jets number

Fig. 13 shows the distribution of the velocity profile on the airfoil surface with two positions of suction at 1 and 4 together. The two indicated suction locations were chosen for two reasons: to treat air sep-



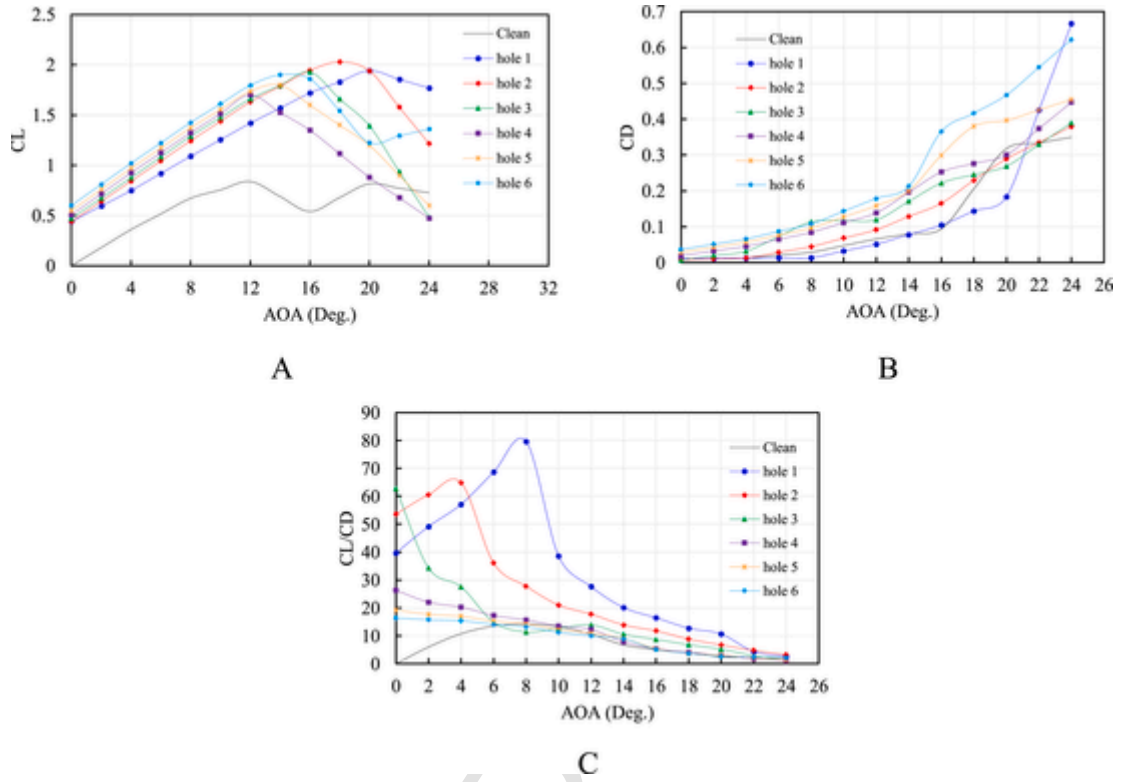


Fig. 10. (A) Lift coefficient, (B) drag coefficient, and (C) lift-to-drag ratio versus AOA at a different hole location compared to clean airfoil.

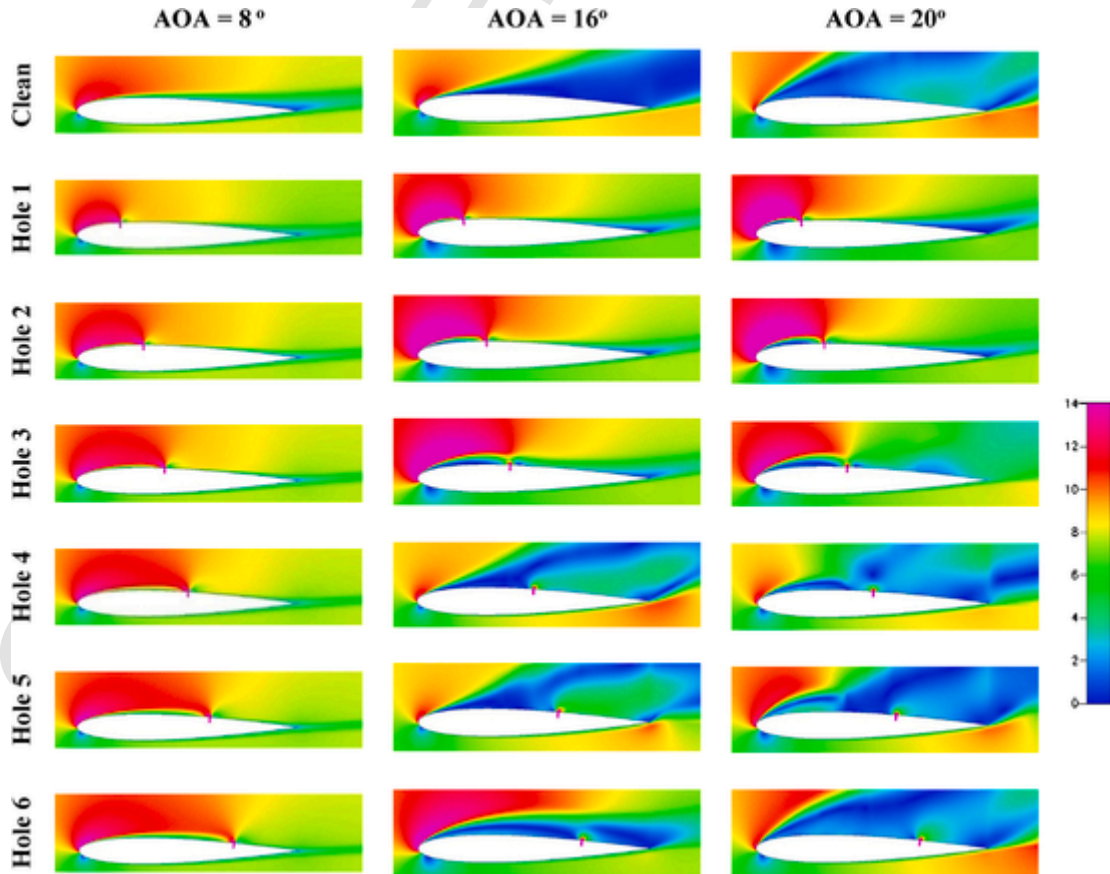


Fig. 11. Velocity contour in (m/s) at a different hole location.

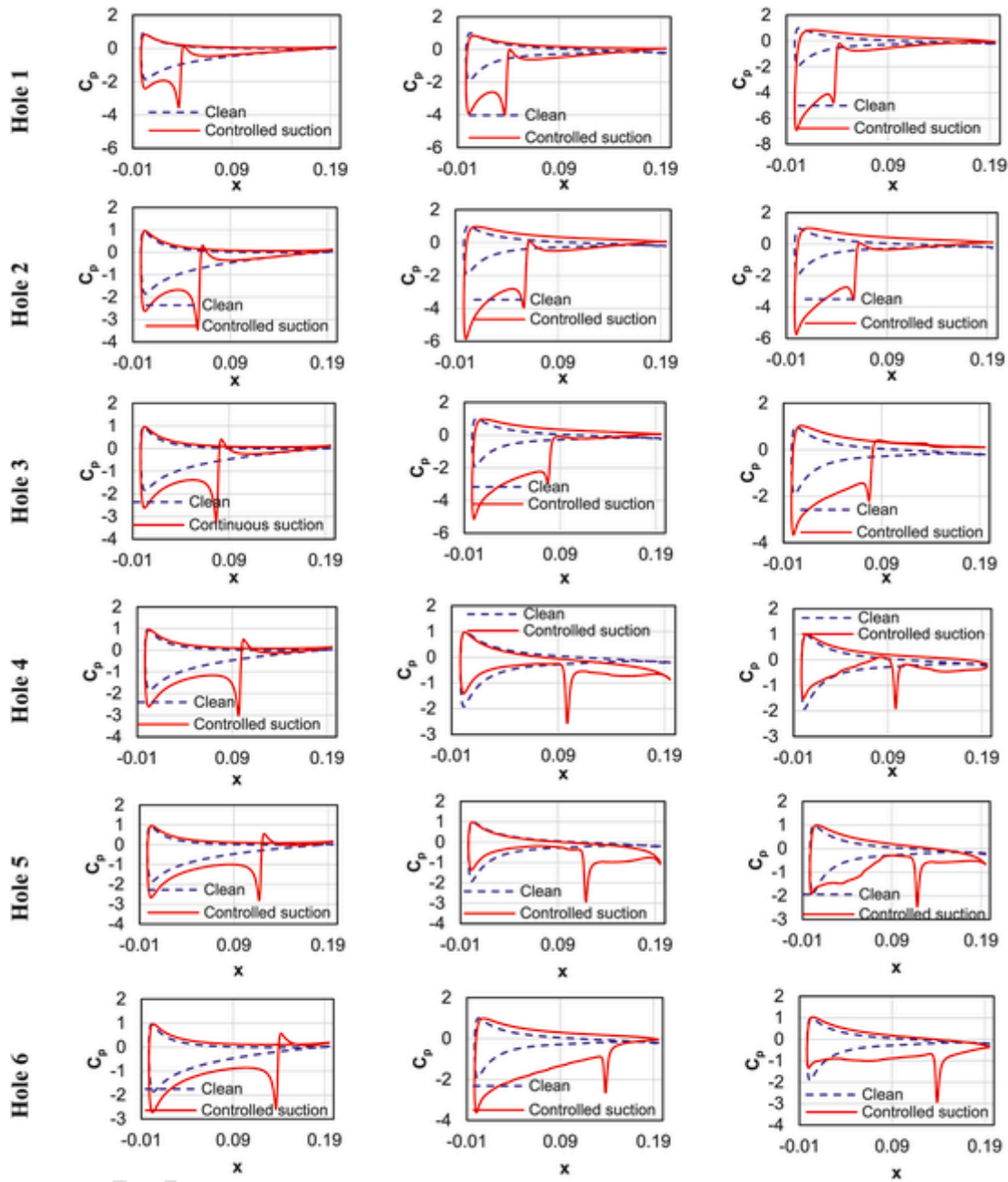


Fig. 12. Pressure coefficient distribution at a different hole location.

variation along the airfoil surface and to improve the lift coefficient over a wider range of angles of attack. As shown in the figure, the choice of the two suction slots succeeded in eliminating the separation from the airfoil surface at angles of attack up to  $16^\circ$ .

To investigate with greater precision, the effect of different suction slot numbers on the flow field surrounding the airfoils 2, 4, and 6, suction slots were selected. Fig. 14 shows a comparison between the different numbers of suction slots with the clean airfoil. It is clear from the results that increasing the number of suction slots with their thoughtful distribution has a positive effect on removing separation up to high angles of attack while ensuring the stability of the flow above the airfoil surface. This results from the boundary layer being ingested more uniformly, restoring the flow to its uniform profile, and not allowing the separation bubble to form even at high angles of attack.

Fig. 15 depicts the pressure coefficient ( $C_p$ ) for clean airfoil and controlled suction cases with different suction slots at AOA equal 8,

16, and  $20^\circ$ . By considering these cases, it was found that abrupt variations in pressure coefficient have been detected at the various suction location. The variation in pressure coefficient has a confident effect on enhancing aerodynamic coefficients such as lift coefficient and lift-to-drag ratio. The pressure coefficient difference  $\Delta C_p$  at the suction location slightly depends on the AOA, and stability (constant value) was observed in all studied cases. The results showed in detail the preference for distributing suction slots on the airfoil suction side as the enclosed area within the curve increases in the pressure coefficient distribution, an increase in the lift coefficient, and the expected improvement in the lift-to-drag ratio. The following was observed by comparing the number of different suction slots at the same angle of attack: Due to the shortening of the separation bubble, the stagnation pressure coefficient steadily increases until it reaches its maximum value when six suction slots are selected.

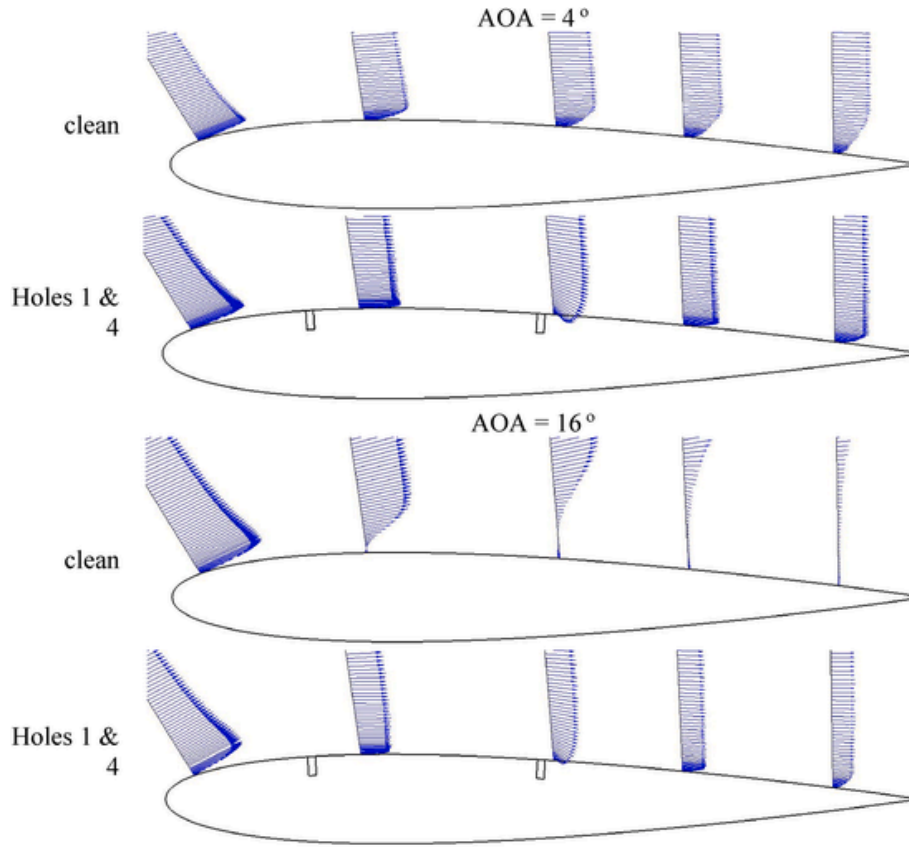


Fig. 13. Boundary layer of two holes compared to clean airfoil.

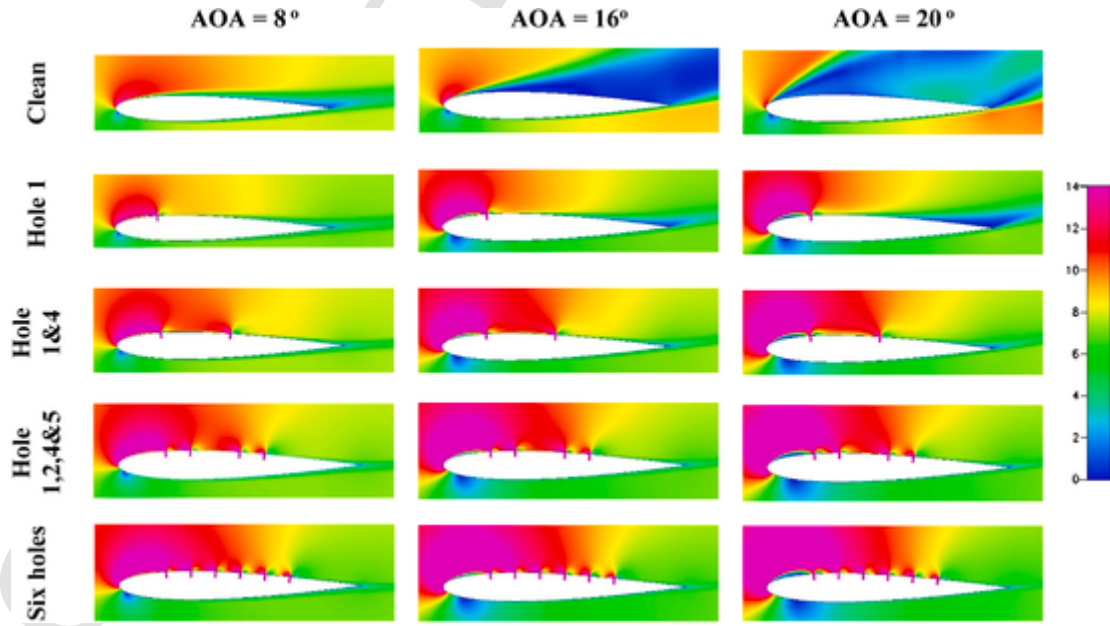


Fig. 14. Velocity contour at different hole numbers.

Fig. 16 shows the change of the lift and drag coefficients and the lift-to-drag ratio as the angles of attack vary for the different numbers of suction slots. The results showed a direct increase of the lift coefficient with the increase in the number of suction slots, where the lift coefficient reached its highest value of 4.8, an increase of 480% compared to clean airfoil at the number of 6 suction slots with an increase in the stall steadily to 22°. While the results showed that when using

2 slots, the stall steadily reached 24° but with a lift coefficient of 2.98. Fig. 16 also showed an increase in the drag coefficient with the increase in the number of suction slots. Regarding the lift-to-drag ratio, the use of two suction slots ensures the highest values associated with the angles of attack, higher than two degrees up to 24°.

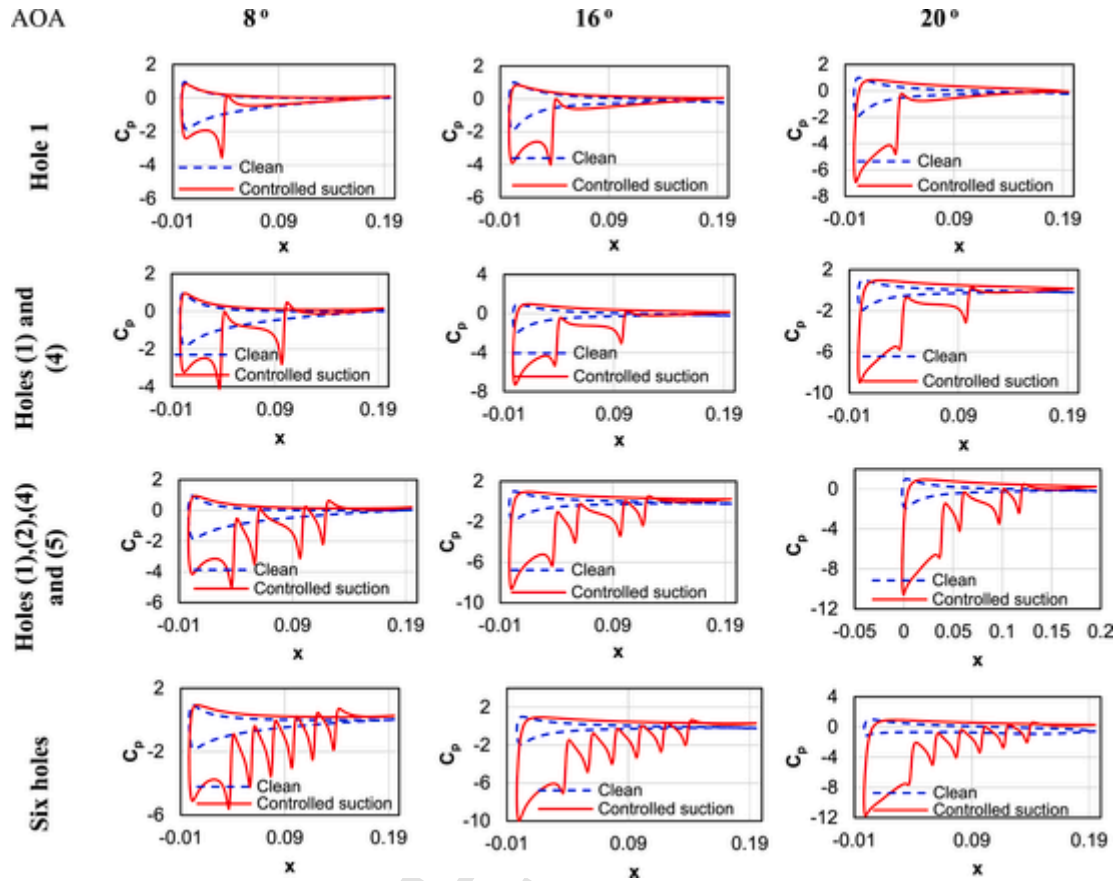


Fig. 15. Pressure coefficient distribution at different hole numbers.

#### 4.3. Effect of suction jets pressure

Studying the effect of suction pressure is of great importance in the current study, as it represents the effective cost of the control technique using suction slots. A detailed study of the suction pressure range from  $-200$  Pa to  $-1400$  Pa. Fig. 17 (A) shows the effect of suction pressure on lift coefficient, drag coefficient, and the lift-to-drag ratio at different angles of attack. The presented results showed an increase in the lift coefficient directly with the suction pressure increase. The stall steadily has a maximum value of  $22^\circ$ . Fig. 17 (B) shows the drag coefficient increase with the suction pressure increase. Fig. 17 (C) shows that the lift-to-drag ratio associated with  $-200$  Pa suction pressure achieved the highest values in the AOA range from  $2$  to  $22^\circ$  compared to other cases.

#### 4.4. Experimental results

In order to validate and prove the success of the proposed study experimentally, a feasible setup was planned to test and realize the suggested technique in an applied manner. The 3D model of current experimental study is built with two side plates to simulate the 2.5D model (infinite wing with side plates). A NACA 0012 three-dimensional squared wing shape was constructed with a  $200$  mm chord and  $200$  mm span. Metal plates with a thickness of  $2$  mm were installed in the tips of the wing to resolve the wing tip vortices developing from the transfer of air from the pressure side to the suction side at non-zero angles of attack. A grid consisting of  $60$  suction holes was made on the wing suction surface. The distribution of suction holes in the form of a  $10 \times 6$  rectangular grid in the direction of span and chord, respectively. The circular shape of the holes with a diameter of  $2$  mm and  $20$  mm distance between the holes were chosen in both spanwise and chordwise directions for ease of application and to ensure uniform airflow from

the suction vents. All ten suction holes are assembled into the suction tube with a diameter of  $8$  mm. The six suction tubes combine with a  $1.2$  mm main tube. The main tube is connected to a plenum chamber set up to maintain a specified pressure less than ambient pressure.

The measurements were conducted under uniform conditions in the ambient environment, the same atmospheric pressure and ambient temperature, inside the Aerodynamics Laboratory of the Institute of Aviation Engineering and Technology. The intake pressure was measured in the branch pipe connected to the ten suction holes with a value of  $1200$  Pa. The measurements were carried out over a wide range of angles of attack from  $0$  to  $24^\circ$  to determine the angles of the stall and the extent of improvement in the lift coefficient and operating range.

The difference between the numerical study while the simulation using CFD, and the experimental investigation of the proposed aerodynamic control technique was considered. The suction was considered as transverse slots with a width equal to the wingspan during the numerical simulation, which is difficult to implement practically now to maintain uniform suction pressure along the wing's span, and the alternative was the circular holes. The percentage of reduction in the suction area must be considered if we maintain the same suction pressure. The amount of suction air governed by the suction pressure and the area of suction holes are the determining factors. Nevertheless, experimental measurements revealed a remarkable improvement that confirms the practical viability of the concept, and it is possible to increase the level of this improvement by developing a suction technique that guarantees a larger area for the suctioned air.

Fig. 18 depicts the measurements of the lift coefficient and drag coefficient measurements in both cases, using and without the aerodynamic control system. The experimental results reported polars include graphical indications on the measurement uncertainty ( $\pm 0.7\%$ ). The characteristic performance parameters of the wing were measured in



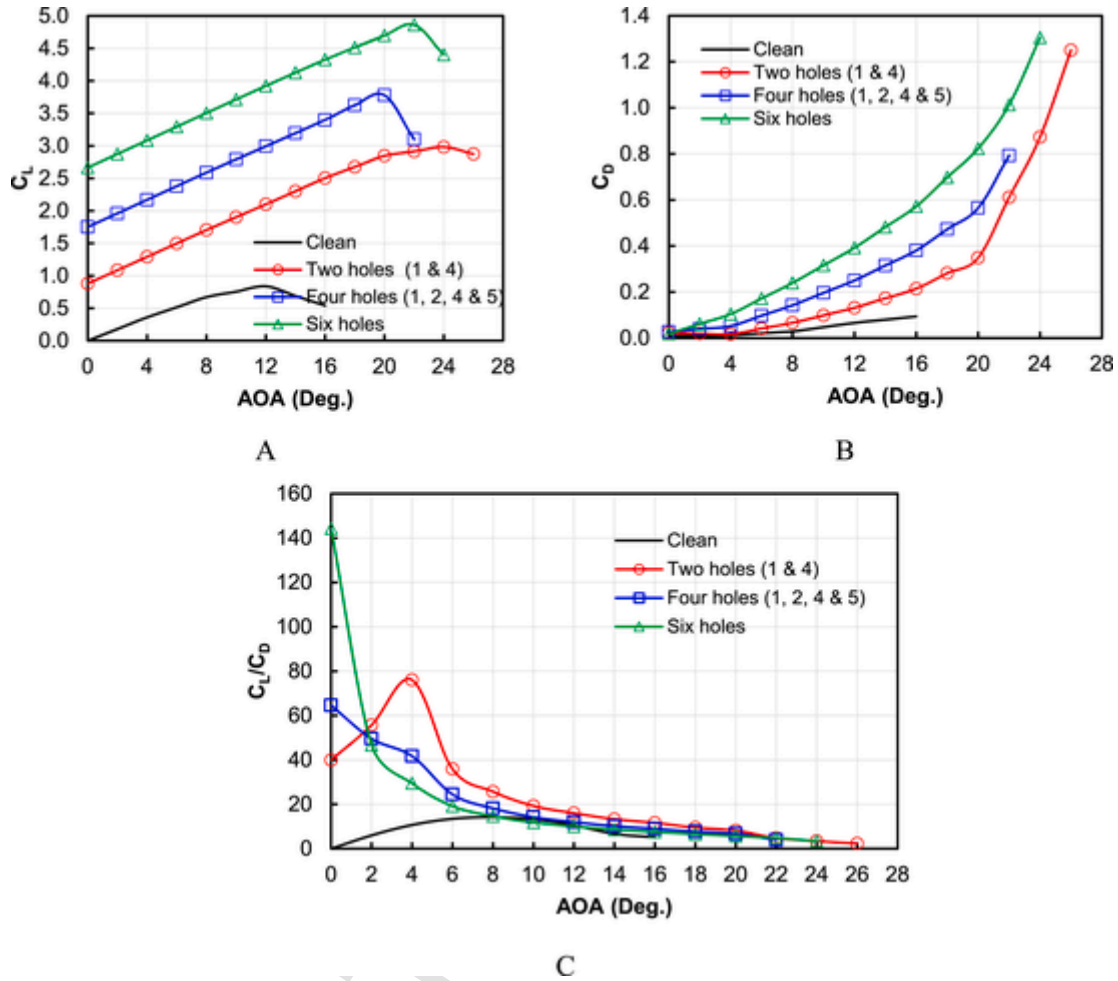


Fig. 16. A Lift coefficient B drag coefficient and C lift to drag ratio versus AOA at different hole numbers compared to clean airfoil.

the range of angles of attack from 0 to 24°, with a step every two degrees. Performance characteristic parameters were measured five times at each AOA. In comparison between the proposed aerodynamic control technique and the original wing, the results showed an increase in the lift coefficient by 0.32 and 0.33 in the range of angles of attack from 0 to 8°, respectively. In contrast, the increase in the highest lift coefficient reached 55.7% at an AOA of 16°. The stall AOA is increased by approximately 4°. Fig. 19 shows the measurements of the drag coefficient, where the results showed the increase in the drag coefficient, which was predicted by the computational results in the numerical simulation.

The suction power is estimated as a function of the suction velocity, which is 34 m/s (at -200 Pa suction pressure). The maximum suction hole numbers (6 holes in chordwise direction  $\times$  50 holes in spanwise direction) for a length of 1 m of the wind turbine blade. For three blades wind turbine the required suction power is about 68 W. The uncontrolled wind turbine power of 1-m frontal area radius, wind speed 8 m/s is about 1000 W [67]. The consumed power ratio is less than 0.07. This ratio is less than the profit power of controlled wind turbine associated with increasing the lift coefficient. The increment in  $C_L$  is about 55% which lead to increase in produced power compared by uncontrolled wind turbine. The lift-to-drag ratio was the most specific parameter that increase the maximum power coefficient for the wind turbine blade [68]. The proper distribution of L/D ratio generates the equal force on the blade section which integrates a stable blade and reduces variation. Equal distribution of L/D ratio on blade radius increased power coefficient by about 15% of other distribution [69].

## 5. Conclusion

Suction jets on the blades of Wind Turbines have a significant impact on their aerodynamic characteristics and, consequently, their power. Current experimental and computational studies examine the effect of hole (slot) location, number, and suction pressure on boundary layer growth, pressure distribution, lift, drag, and lift-to-drag performance. The following points can be used to summarize the findings.

- The elimination of boundary layers by active suction stabilizes the flow velocity of the boundary layer and eventually retains a laminar boundary layer.
- The suction close to the trailing edge demonstrates the best results in the lift coefficient up to AOA equals 14°.
- The suction close to maximum thickness shows an increase in the lift coefficient for AOA ranging from 14 to 20°.
- Increasing the number of suction slots with their thoughtful distribution has a positive effect on removing separation up to high angles of attack.
- There is a direct increase in the lift coefficient with the number of suction slots up to 480% compared to clean airfoil.
- There is an increase in the lift coefficient with the suction pressure increase, but this represents the cost of the control technique using suction slots.
- The lift-to-drag ratio associated with -200 Pa suction pressure achieved the highest values in the AOA range from 2 to 22° compared to other cases.

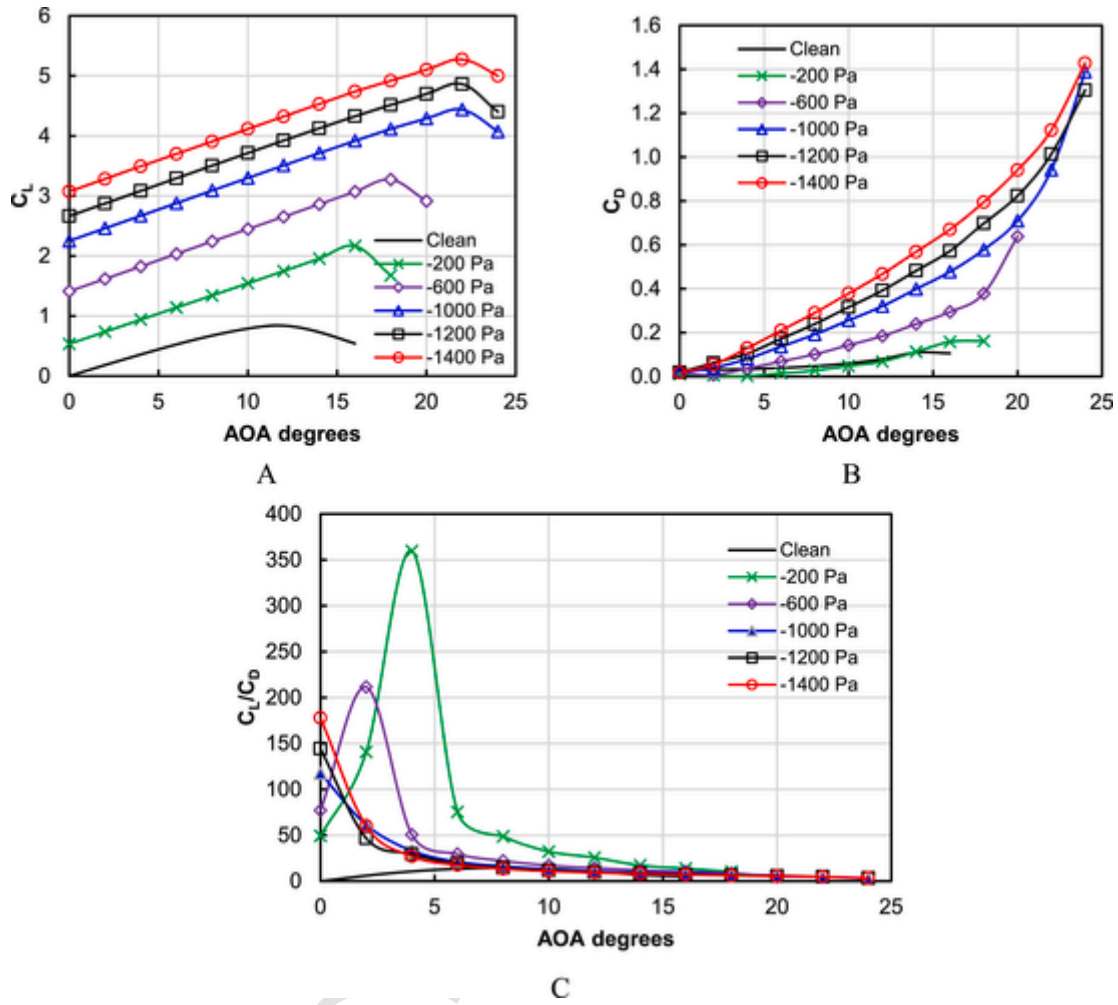


Fig. 17. (A) Lift coefficient, (B) drag coefficient, and (C) lift-to-drag ratio versus AOA at different suction pressure compared to clean airfoil.

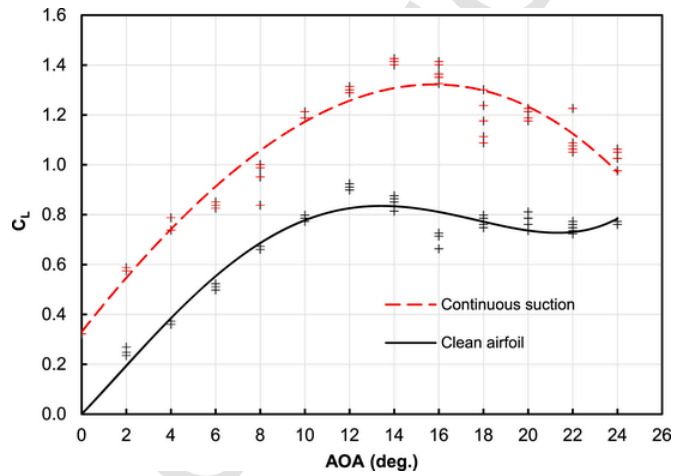


Fig. 18. Lift coefficient versus AOA with controlled suction compared to clean airfoil.

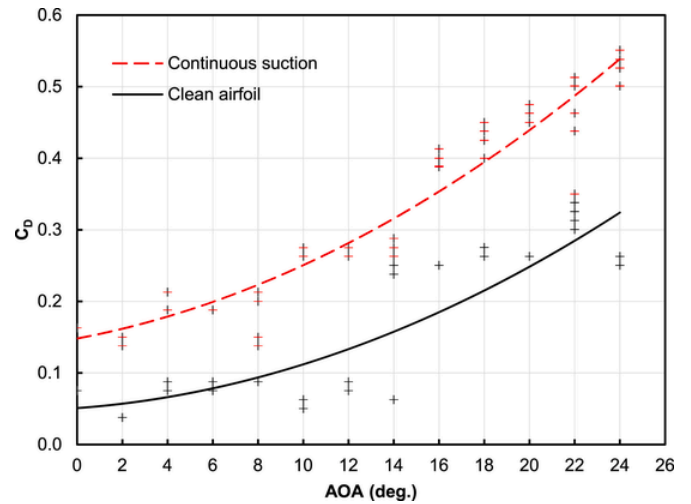


Fig. 19. Drag coefficient versus AOA with controlled suction compared to clean airfoil.

- The experimental results showed an increase in the lift coefficient by 0.32–0.33 in the range of angles of attack from 0 to 8°, respectively, using six holes instead of a slot along the span length.
- The experimental results demonstrated a 55.7% increase in the maximum lift coefficient at 16° AOA.

- The stall AOA is increased by approximately  $4^\circ$  by introducing suction flow control compared to clean airfoil using the experimental investigation.

#### Authorship contribution statement

**Ahmed M. Elsayed:** Investigation, Visualization, Validation, laboratory experiments, writing methodology, **Mohamed A. Khalifa:** Laboratory experiments, Investigation, Data curation, writing methodology, **Ernesto Benini:** Methodology, Investigation, **Mohamed. A. Aziz:** Conceptualization, writing methodology, labora-

tory experiments, Investigation, Supervision, Project administration, Writing, the main search's idea.

#### Declaration of competing interest

The authors declare that they have no known competing financial interests or personal relationships that could have appeared to influence the work reported in this paper.

#### Data availability

Data will be made available on request.

#### Nomenclature

$C_L$	Lift coefficient
$C_D$	Drag coefficient
$C_p$	Pressure coefficient
$e$	Specific internal energy (per unit mass) (J/kg)
$F$	Body force, (N)
$k$	Thermal conductivity (W/m <sup>2</sup> °C)
$\dot{m}$	Mass flow rate, kg/s
$P$	Pressure (N/m <sup>2</sup> )
$Q$	Internal heat generation (J/m <sup>3</sup> )
$q_r$	Radiation heat flux vector (W/m <sup>2</sup> )
$T$	Temperature, (K)
$U$	Velocity, (m/s)
$\vec{V}$	Velocity vector, (m/s)
$\rho$	Air density, (kg/m <sup>3</sup> )
$\mu$	Viscosity (Pa s)
$\lambda$	Second coefficient of viscosity ( $\lambda = -\frac{2}{3}\mu$ for a monatomic gas)
$\zeta$	Another second coefficient of viscosity defined in terms of $\lambda$ as $\zeta = \lambda + \frac{2}{3}\mu$ . For a monatomic gas, $\zeta = 0$
$\Phi$	Mechanical or viscous dissipation function (W/m <sup>3</sup> )

#### References

- [1] IRENA. Geothermal energy capacities. Renewable capacity statistics 2017. Abu Dhabi: International Renewable Energy Agency; 2017. ISBN 978-92-9260-018-1.
- [2] Aramendia I, Fernandez-Gamiz U, Ramos-Hernanz J.A. Flow control devices for wind turbines energy harvesting and energy efficiency. Lect Notes Eng 2017;37. <https://doi.org/10.1007/978-3-319-49875-1>.
- [3] Rezaeiha Abdolrahim, Hamid Montazeri, Blocken Bert. Active flow control for power enhancement of vertical axis wind turbines: leading-edge slot suction. Energy 2019;189:116131. <https://doi.org/10.1016/j.energy.2019.116131>.
- [4] Xu Kewei, Zha Gecheng. Investigation of coflow jet active flow control for Wind Turbine airfoil. In: AIAA aviation 2020 forum; 2020. p. 2942. <https://doi.org/10.2514/6.2020-2942>.
- [5] Zhu Haitian, Hao Wenxing, Chun Li, Ding Qinwei, Wu Baihui. Application of flow control strategy of blowing, synthetic and plasma jet actuators in vertical axis Wind Turbines. Aero Sci Technol 2019;88:468–80. <https://doi.org/10.1016/j.ast.2019.03.022>.
- [6] Maleki Gholam Hossein, Davari Ali Reza, Reza Soltani Mohammad. Experimental investigation of the effect of active flow control on the wake of a Wind Turbine blade. Proc IME C J Mech Eng Sci 2021;235(22):6122–38. <https://doi.org/10.1177/09544062211008932>.
- [7] Shi Fangrui, Xu Yingqiao, Sun Xiaojing. Numerical investigation of active flow control with co-flowing jet in a horizontal axis Wind Turbine. Wind Eng 2021;45(5):1101–22. <https://doi.org/10.1177/0309524X20961394>.
- [8] Aziz Mohamed A, Elsayed Ahmed M. CFD based optimization of active flow control. In: Twelfth international conference of fluid dynamics (ICFD12); December 2016. p. 19–20. Cairo, EGYPT.
- [9] Xu Kewei, Zha Gecheng. High efficiency Wind Turbine using co-flow jet active flow control. In: Turbo expo: power for land, sea, and air, vol. 84898. American Society of Mechanical Engineers; 2021. <https://doi.org/10.1115/GT2021-59664.V001T40A003>.
- [10] Ali Boudis, Ouahiba Guerri, Hamid Oualli, Ahmed Benzaoui. Aerodynamic optimization of active flow control over S809 airfoil using synthetic jet. In: 2018 international conference on wind energy and applications in Algeria (ICWEAA). IEEE; 2018. p. 1–6. <https://doi.org/10.1109/ICWEAA.2018.8605084>.
- [11] Botero Nicolas, Ratkovich Nicolas, Santiago Lain, Omar D, Lopez Mejia. Synthetic jets as a flow control device for performance enhancement of vertical axis hydrokinetic turbines: a 3D computational study. Heliyon 2022;e10017. <https://doi.org/10.1016/j.heliyon.2022.e10017>.
- [12] Rice Thomas T, Taylor Keith, Amitay Michael. Wind tunnel quantification of dynamic stall on an S817 airfoil and its control using synthetic jet actuators. Wind Energy 2019;22(1):21–33. <https://doi.org/10.1002/we.2266>.
- [13] Govindan Srinivasa Sudharsan, Santiago Arockia Edwin Xavier. Optimized dielectric barrier discharge-plasma actuator for active flow control in Wind Turbine. Struct Control Health Monit 2019;26(12):e2454. <https://doi.org/10.1002/stc.2454>.
- [14] Ebrahimi Abbas, Zare Majid. Active flow control in darrieus wind turbine blade using plasma actuator. Sharif J Mech Eng 2022. <https://doi.org/10.24200/J40.2022.59189.1623>.
- [15] Guoqiang Li, Zhang Weiguo, Jiang Yubiao, Yang Pengyu. Experimental investigation of dynamic stall flow control for Wind Turbine airfoils using a plasma actuator. Energy 2019;185:90–101. <https://doi.org/10.1016/j.energy.2019.07.017>.
- [16] Guoqiang Li, Yi Shihe. Large eddy simulation of dynamic stall flow control for Wind Turbine airfoil using plasma actuator. Energy 2020;212:118753. <https://doi.org/10.1016/j.energy.2020.118753>.
- [17] Aziz M.A, Elsayed A.M. Numerical investigation and optimization of airfoil flow control using passive air-jet. Thermophys Aeromechanics 2019;26(3):361–74. <https://doi.org/10.1134/S0869864319030053>.
- [18] Acarer Sercan. Peak lift-to-drag ratio enhancement of the DU12W262 airfoil by passive flow control and its impact on horizontal and vertical axis Wind Turbines. Energy 2020;201:117659. <https://doi.org/10.1016/j.energy.2020.117659>.
- [19] Negi Pankaj, Subhash Maharshi. Method to control flow separation over Wind Turbine blade: a CFD study. Mater Today Proc 2021;46:10960–3. <https://doi.org/10.1016/j.matpr.2021.02.040>.
- [20] Ni Zao, Dhanak Manhar, Su Tsung-chow. Improved performance of a slotted blade using a novel slot design. J Wind Eng Ind Aerod 2019;189:34–44. <https://doi.org/10.1016/j.jweia.2019.03.018>.
- [21] Zhu Haitian, Hao Wenxing, Chun Li, Ding Qinwei, Wu Baihui. A critical study on passive flow control techniques for straight-bladed vertical axis Wind Turbine. Energy 2018;165:12–25. <https://doi.org/10.1016/j.energy.2018.09.072>.
- [22] Zhu Chengyong, Chen Jie, Wu Jianghai, Wang Tongguang. Dynamic stall control

- of the Wind Turbine airfoil via single-row and double-row passive vortex generators. *Energy* 2019;189:116272. <https://doi.org/10.1016/j.energy.2019.116272>.
- [23] Zhu Chengyong, Qiu Yingning, Feng Yanhui, Wang Tongguang, Li Hui. Combined effect of passive vortex generators and leading-edge roughness on dynamic stall of the Wind Turbine airfoil. *Energy Convers Manag* 2022;251: 115015. <https://doi.org/10.1016/j.enconman.2021.115015>.
- [24] Zhu Chengyong, Wang Tongguang, Chen Jie, Zhong Wei. Effect of single-row and double-row passive vortex generators on the deep dynamic stall of a Wind Turbine airfoil. *Energies* 2020;13(10):2535. <https://doi.org/10.3390/en13102535>.
- [25] Mereu Riccardo, Passoni Stefano, Inzoli Fabio. Scale-resolving CFD modeling of a thick Wind Turbine airfoil with application of vortex generators: validation and sensitivity analyses. *Energy* 2019;187:115969. <https://doi.org/10.1016/j.energy.2019.115969>.
- [26] Mostafa Wafaa, Abdelsamie Abouelmagd, Sedrak Momtaz, Thévenin Dominique, Mohamed Mohamed H. Quantitative impact of a micro-cylinder as a passive flow control on a horizontal axis Wind Turbine performance. *Energy* 2022;244:122654. <https://doi.org/10.1016/j.energy.2021.122654>.
- [27] Shi Xuyang, Xu Shuai, Ding Li, Huang Diangu. Passive flow control of a stalled airfoil using an oscillating micro-cylinder. *Comput Fluids* 2019;178:152–65. <https://doi.org/10.1016/j.compfluid.2018.08.012>.
- [28] Mostafa W, Abdelsamie A, Mohamed M, Thévenin D, Sedrak M. Aerodynamic performance improvement using a micro-cylinder as a passive flow control around the S809 airfoil. In: IOP conference series: materials science and engineering, vol. 973. IOP Publishing; 2020. p. 12040. <https://doi.org/10.1088/1757-899X/973/1/012040>, no. 1.
- [29] Aboelezz Ahmed, Ghali Hani, Gamal Elbayomi, Madboli Mohamed. A novel VAWT passive flow control numerical and experimental investigations: guided vane airfoil wind turbine. *Ocean Eng* 2022;257:111704. <https://doi.org/10.1016/j.oceaneng.2022.111704>.
- [30] New D.T, Ng Bing Feng. Flow control through bio-inspired leading-edge tubercles. Cham: Springer; 2020. <https://doi.org/10.1007/978-3-030-23792-9>.
- [31] Benavides Zadorozhna D, Benavides O, Sierra Grajeda J, Figueroa Ramirez S, de la Cruz May L. A parametric study of the effect of leading edge spherical tubercle amplitudes on the aerodynamic performance of a 2D Wind Turbine airfoil at low Reynolds numbers using computational fluid dynamics. *Energy Rep* 2021;7: 4184–96. <https://doi.org/10.1016/j.eegy.2021.06.093>.
- [32] Supreeth R, Arokiaswamy A, Anirudh K, Pradyumna R.K, Pramod P.K, Sanarahamat A.K. Experimental and numerical investigation of the influence of leading edge tubercles on S823 airfoil behavior. *J Appl Fluid Mech* 2020;13(6): 1885–99. <https://doi.org/10.47176/JAFM.13.06.31244>.
- [33] Mishra Alok, Ashoke De. Investigation of passive flow control over an airfoil using leading edge tubercles. *arXiv* 2021. <https://doi.org/10.48550/arXiv.2103.08854>, preprint arXiv:2103.08854.
- [34] Saenz-Aguirre Aitor, Fernandez-Gamiz Unai, Zulueta Ekaitz, Ulazia Alain, Martinez-Rico Jon. Optimal Wind Turbine operation by artificial neural network-based active gurney flap flow control. *Sustainability* 2019;11(10):2809. <https://doi.org/10.3390/su11102809>.
- [35] Aramendia Inigo, Saenz-Aguirre Aitor, Fernandez-Gamiz Unai, Zulueta Ekaitz, Lopez-Guede Jose Manuel, Boyano Ana, et al. Gurney flap implementation on a DU91W250 airfoil. *Multidiscip Digit Publ Instit Proc* 2018;2(23):1448. <https://doi.org/10.3390/proceedings2231448>.
- [36] Hao Wenxing, Bashir Musa, Chun Li, Sun Chengda. Flow control for high-solidity vertical axis Wind Turbine based on adaptive flap. *Energy Convers Manag* 2021; 249:114845. <https://doi.org/10.1016/j.enconman.2021.114845>.
- [37] Bartholomay Sirko, Michos Grigoris, Perez-Becker Sebastian, George Pechlivanoglou, Nayeri Christian, Nikolaou Grigoris, et al. Towards active flow control on a research scale Wind Turbine using pid controlled trailing edge flaps. In: 2018 Wind energy symposium; 2018. p. 1245. <https://doi.org/10.2514/6.2018-1245>.
- [38] Güler Emre, Durhasan Tahir, Karasu Ilyas, Akbiyik Hurrem. Passive flow control around NACA 0018 airfoil using riblet at low Reynolds number. *J Instit Sci Technol* 2021;11(3):2208–17. <https://doi.org/10.21597/jist.897982>.
- [39] Tiainen Jonna, Aki Grönman, Jaatinen-Värrä Ahti, Pyy Lauri. Effect of non-ideally manufactured riblets on airfoil and Wind Turbine performance. *Renew Energy* 2020;155:79–89. <https://doi.org/10.1016/j.renene.2020.03.102>.
- [40] Wang Longjun, Alam Md Mahbub, Rehman Shafiqur, Zhou Yu. Effects of blowing and suction jets on the aerodynamic performance of Wind Turbine airfoil. *Renew Energy* 2022. <https://doi.org/10.1016/j.renene.2022.06.126>.
- [41] Sun Jinjing, Huang Diangu. Numerical investigation of boundary layer suction control positions on airfoils for vertical-axis Wind Turbine. *J Mech Sci Technol* 2021;35(7):2903–14. <https://doi.org/10.1007/s12206-021-0614-0>.
- [42] Ohashi Masahiro, Morita Yuki, Hirokawa Shiho, Fukagata Koji, Tokugawa Naoko. Parametric study toward optimization of blowing and suction locations for improving lift-to-drag ratio on a Clark-Y airfoil. *J Fluid Sci Technol* 2020;15(2). <https://doi.org/10.1299/jfst.2020jfst0008>. JFST0008-JFST0008.
- [43] Huang Luana, Huang P.G, LeBeau R.P, Hauser Th. Numerical study of blowing and suction control mechanism on NACA0012 airfoil. *J Aircraft* 2004;41(5): 1005–13. <https://doi.org/10.2514/1.2255>.
- [44] Sogukpinar Haci. The effects of NACA 0012 airfoil modification on aerodynamic performance improvement and obtaining high lift coefficient and post-stall airfoil. In: AIP conference proceedings, vol. 1935. AIP Publishing LLC; 2018. p. 20001. <https://doi.org/10.1063/1.5025955>, no. 1.
- [45] Gul M, Uzol O.G.U.Z, Akmandor I.S. An experimental study on active flow control using synthetic jet actuators over S809 airfoil. *J Phys Conf* 2014;524(1): 012101. <https://doi.org/10.1088/1742-6596/524/1/012101>. IOP Publishing.
- [46] Esmael Fatahian, Fatahian Hossein. Simultaneous effect of suction and cavity for controlling flow separation on NACA 0012 airfoil-CFD approach. *Gazi Univ J Sci* 2021;34(1):235–49. <https://doi.org/10.35378/gujs.706052>.
- [47] Fatahian Esmael, Nichkoobi Ali Lohrasbi, Salarian Hesamoddin, Khaleghinia Jahanfar. Comparative study of flow separation control using suction and blowing over an airfoil with/without flap. *Sādhanā* 2019;44(11):1–19. <https://doi.org/10.1007/s12046-019-1205-y>.
- [48] Bak Khoshnevis, Abdolamir Shima Yazdani, Salimipour Erfan. Effects of CFJ flow control on aerodynamic performance of symmetric NACA airfoils. *J Turbul* 2020; 21(12):704–21. <https://doi.org/10.1080/14685248.2020.1845911>.
- [49] Atzori Marco, Vinuesa Ricardo, Fahland Georg, Alexander Stroh, Gatti Davide, Frohnappell Bettina. Aerodynamic effects of uniform blowing and suction on a NACA4412 airfoil. *Flow, Turbul Combust* 2020;105(3):735–59. <https://doi.org/10.1007/s10494-020-00135-z>.
- [50] Arunraj R, Logesh K, Balaji V, Ravichandran T, Yuvashree G.K. Experimental investigation of lift enhancement by suction-assisted delayed separation of the boundary layer on NACA 0012 airfoil. *Int J Ambient Energy* 2019;40(3):243–7. <https://doi.org/10.1080/01430750.2017.1386127>.
- [51] Zahedi R, Ahmadi A, Sadeh M. Investigation of the load management and environmental impact of the hybrid cogeneration of the wind power plant and fuel cell. *Energy Rep* 2021;7:2930–9. <https://doi.org/10.1016/j.eegy.2021.05.008>.
- [52] Zahedi R, Rad A.B. Numerical and experimental simulation of gas-liquid two-phase flow in 90-degree elbow. *Alex Eng J* 2022;61(3):2536–50. <https://doi.org/10.1016/j.aej.2021.07.011>.
- [53] Yousefi Kianoosh, Saleh Reza. Three-dimensional suction flow control and suction jet length optimization of NACA 0012 wing. *Meccanica* 2015;50(6): 1481–94. <https://doi.org/10.1007/s11012-015-0100-9>.
- [54] Elsayed Ahmed M. Design optimization of diffuser augmented wind turbine. *CFD Lett* 2021;13(8):45–59. <https://doi.org/10.37934/cfdl.13.8.4559>.
- [55] Aziz M.A, Owis Farouk M, Abdelrahman M.M. Preliminary design of a transonic fan for a low by-pass turbofan engine. *Int Rev Aerospace Eng* 2013;6(2):114–27.
- [56] Elsayed Ahmed M, Owis Farouk M, Madbouli Abdel Rahman M. Numerical computation and optimization of turbine blade film cooling. *Adv Mech Eng* 2014;6: 2014–528031. <https://doi.org/10.1155/2014.528031>.
- [57] Elsayed Ahmed M, Owis Farouk M, Madbouli Abdel Rahman M. Film cooling optimization using numerical computation of the compressible viscous flow equations and simplex algorithm. *Int J Aerospace Eng* 2013;2013. <https://doi.org/10.1155/2013/859465>.
- [58] Aziz M.A, Owis Farouk M, Abdelrahman M.M. Design optimization of a transonic-fan rotor using numerical computations of the full compressible Navier-Stokes equations and simplex algorithm. *Int J Rotating Mach* 2014;(2014). <https://doi.org/10.1155/2014/743154>.
- [59] Elsayed Ahmed M, Elbanna Hesham M, Abdelrahman M.M. Design optimization of thrust augmentation ejector utilizing the CFD tools. In: *Proceedings of ICFD10*; 2010.
- [60] Aziz Mohamed A, Elbanna Hesham, Abdulrahman Mohamed M. High fidelity design optimization of a three dimension supersonic intake. In: 43rd AIAA fluid dynamics conference; 2013. p. 2462. <https://doi.org/10.2514/6.2013-2462>.
- [61] Aziz Mohamed A, Gaheen Osama A. Effect of the isothermal fins on the natural convection heat transfer and flow profile inside a vertical channel with isothermal parallel walls. *SN Appl Sci* 2019;1(10):1–13. <https://doi.org/10.1007/s42452-019-1232-7>.
- [62] Aziz Mohamed A, Elsayed Ahmed M. Thermofluid effects of solar chimney geometry on performance parameters. *Renew Energy* 2022;200:674–93. <https://doi.org/10.1016/j.renene.2022.10.022>.
- [63] Elsayed Ahmed M, Aziz Mohamed A. CFD Investigations for UAV and MAV low speed Airfoils characteristics. *Int Rev Aerospace Eng (I. RE. AS. E)* 2015;8(3). ISSN 1973-7459.
- [64] Elsayed Ahmed M, Farghaly Mohamed B. Theoretical and numerical analysis of vortex bladeless wind turbines. *Wind Eng* 2022. <https://doi.org/10.1177/0309524X221080>. 0309524X221080468.
- [65] El-Salamony, Mostafa E, Aziz Mohamed A. Impact of N-shaped wing morphing on solar-powered aircraft. *Unmanned Syst* 2021;9(4):309–20. <https://doi.org/10.1142/S2301385021500138>.
- [66] Rinoie Kenichi, Okuno Masafumi, Sunada Yasuto. Airfoil stall suppression by use of a bubble burst control plate. *AIAA J* 2009;47(2):322–30. <https://doi.org/10.2514/1.37352>.
- [67] Mathew Sathyajith. *Wind energy: fundamentals, resource analysis and economics*. vol. 1. Berlin: Springer; 2006.
- [68] Yass A.R, Muhammad, Rasheed Majeed, Raghad, Amer Hamad Muhiesan. Contribution of lift-to-drag ratio on power coefficient of HAWT blade for different cross-sections. *Open Eng* 2022;12(1):716–28. <https://doi.org/10.1515/eng-2022-0324>.